J. Fluid Mech. (2003), *vol.* 489, *pp.* 29–54. © 2003 Cambridge University Press
DOI: 10.1017/S0022112003005160 Printed in the United Kingdom

Particle clouds in homogeneous and stratified environments

By JOHN W. M. BUSH, B. A. THURBER AND F. BLANCHETTE

Department of Mathematics, Massachusetts Institute of Technology, 77 Massachusetts Avenue, Cambridge, MA 02139, USA

(Received 14 March 2001 and in revised form 7 March 2003)

We examine the settling of monodisperse heavy particles released into a fluid when the resulting motion is sufficiently vigorous that the particle cloud initially assumes the form of a turbulent thermal. A laboratory study is complemented by numerical simulations of particle cloud dynamics in both homogeneous and stratified ambients. In the homogeneous ambient, the cloud generated by a total buoyancy excess $Q = g'N_pV_p$, where g' is the reduced gravity of the N_p spherical particles of volume $V_p = 4\pi a^3/3$, evolves in a manner consistent with a classical fluid thermal. The cloud grows through turbulent entrainment and decelerates until its speed is exceeded by that of the individual particles w_s, at which point the particles rain out as individuals. For particle Reynolds numbers $Re_p = w_s a/\nu$ in the range of 0.1–300, the fallout height Z_f is found to be $Z_f/a = (11 \pm 2)(Q^{1/2}/(w_s a))^{0.83}$. For high Re_p particles, the fallout height assumes the simple form: $Z_f/a = (9 \pm 2)N_p^{1/2}$. Following fallout, the particles sink at their individual settling speeds in the form of a bowl-shaped swarm. In a stratified environment characterized by a constant Brunt–Väisälä frequency N, the mode of fallout depends explicitly on the stratified cloud number, $N_s = w_s Q^{-1/4} N^{-1/2}$. For $N_s < 1$, the cloud overshoots, rebounds past, then intrudes at the neutral height, Z_N, of the equivalent fluid thermal. The particles fall out between the depth of maximum penetration and the spreading neutral cloud, and may be distributed over a relatively broad area. For $N_s > 1$, the particles fall out in the form of a bowl-shaped swarm at a height $Z_f < Z_N$, thus giving rise to a relatively localized deposit. For $N_s > 4$, the fallout height is largely uninfluenced by the stratification and is adequately described by the homogeneous result. Regardless of N_s, following particle fallout in a stratified ambient, the fluid entrained by the thermal ascends and intrudes at a rebound height given to leading order by $3Z_f/4$. Criteria for three distinct modes of particle deposition in a stratified ambient are developed.

1. Introduction

An ability to predict the mixing processes accompanying particle settling in the aqueous environment is of significant environmental interest. The instantaneous release of heavy particles into homogeneous or stratified fluids arises in a number of geophysical and industrial settings, including the discharge of dredged materials and industrial waste into rivers, lakes and oceans (Bühler & Papantoniou 1999). Where the waste is contaminated, it is important to understand the fate of both the solid waste, and the fluid with which it interacts. The case of instantaneous particle release considered here is an example of a broader class of problems in environmental fluid

dynamics concerning mixing by spatially localized releases of a buoyant or negatively buoyant second phase, either bubbles, drops or particles (Socolofsky, Crounse & Adams 1999).

If the motion of an isolated mass of buoyant fluid is sufficiently vigorous, specifically, if the Reynolds number based on its characteristic radius R, speed U and viscosity ν, $Re = UR/\nu > 1000$, the cloud will rise as a turbulent thermal. The dynamics of turbulent fluid thermals driven by a small density difference between source fluid and ambient have been studied extensively (Scorer 1957; Turner 1973). A buoyant thermal grows by turbulent entrainment, so that its radius increases linearly with distance from the source, while the density difference between thermal and ambient decreases (Morton, Taylor & Turner 1956). The evolution of a turbulent thermal in a homogeneous ambient may be uniquely prescribed by its mean distance z from the source and its total buoyancy, $Q = g(\rho_0 - \rho)V_0/\rho_0$, where ρ and V_0 are the initial density and volume of the source fluid and ρ_0 is the density of the ambient. Dimensional considerations indicate that the thermal half-width b, speed U and buoyancy $g' = g(\rho_0 - \rho)/\rho_0$ must evolve according to

$$b = \alpha z, \quad U \sim Q^{1/2}/z, \quad g' \sim Q/z^3. \tag{1.1}$$

The quantities may alternatively be expressed in terms of time t since release as

$$b \sim Q^{1/4}t^{1/2}, \quad U \sim Q^{1/4}t^{-1/2}, \quad g' \sim Q^{1/4}t^{-3/2}. \tag{1.2}$$

Scorer (1957) confirmed that the thermal width grows linearly with distance from the source, and measured entrainment coefficients between 0.2 and 0.34 with a mean of $\alpha = 0.25$. Richards (1961) reported values between 0.13 and 0.53, and Woodward (1959) reported a mean value of 0.27. A buoyant thermal rises indefinitely in a homogeneous environment; however, in a stratified environment, the thermal buoyancy is continually reduced until the thermal stops rising and intrudes at its level of neutral buoyancy, Z_N, in the form of an axisymmetric gravity current. For the case of a uniformly stratified fluid characterized by a constant Brunt–Väisälä frequency, $N = ((g/\rho_0)(\mathrm{d}\rho/\mathrm{d}z))^{1/2}$, dimensional considerations indicate that the intrusion height must vary as

$$Z_N = C_1 \frac{Q^{1/4}}{N^{1/2}}. \tag{1.3}$$

The experimental study of Morton *et al.* (1956) indicates a coefficient of $C_1 = 2.6 \pm 0.4$ for the mean height of neutral clouds resulting from Boussinesq fluid thermals.

This simple physical picture of a pure Boussinesq thermal is altered if the density difference between thermal and ambient is large, or if the thermal has significant initial momentum. Papantoniou, Bühler & Dracos (1990) examined the dynamics of thermals and momentum puffs, and demonstrated that an increase in the initial momentum of a thermal results in diminished entrainment. Maxworthy (1974, 1977) presents detailed experimental studies of turbulent and laminar vortex rings, which represent the limit of thermals with no buoyancy. Escudier & Maxworthy (1973) considered the influence of added mass on the dynamics of thermals and demonstrated that the growth rate is expected to depend explicitly on the density difference between thermal and ambient $\Delta\rho$. For practical ranges of $\Delta\rho/\rho$, their theory indicates that the asymptotic linear thermal growth will be achieved after a distance of no more than 10 times the initial thermal radius. Their theory, however, presumes that the entrainment rate into the thermal, α, is constant. Baines & Hopfinger (1984) derive a modified entrainment

law for non-Boussinesq thermals, and demonstrate that such heavy sinking thermals expand more rapidly than do their Boussinesq counterparts. Thus, one expects a relatively rapid approach to Boussinesq behaviour (over approximately four initial cloud diameters). However, they also observe experimentally a delayed onset of vortex generation after exit for the case of heavy thermals. This physical picture of thermal motion is further complicated when the buoyancy is associated with the presence of rigid particles.

Slack (1963) pointed out that a cloud of particles in air may settle at a rate significantly larger than that of the individual particles. For sufficiently large numbers of small particles, the cloud behaves as a second phase of fluid, and so takes the form of a negatively buoyant turbulent thermal. He also observed that at a critical distance from the source, termed the fallout height, the particles fall out of the base of the descending thermal in the form of a bowl-shaped swarm which descends at the settling speed of the individual particles. The ability of particle clouds to behave as a second phase of fluid in which the particles are effectively in dilution rather than in suspension was used by Bradley (1965) to account for the anomalous settling rates observed in sedimentation in lakes.

Rahimipour & Wilkinson (1992) examined turbulent particle clouds comprised of monodisperse particles with a limited range of particle Reynolds numbers ($1 < Re_p < 10$). The dynamics of a cloud of buoyancy $Q = (\rho_p - \rho) g N_p V_p / \rho$ and radius b initially consisting of N_p particles of density ρ_p and volume V_p with settling speed w_s released into a fluid of density ρ was characterized in terms of a cloud number $N_c = w_s b Q^{-1/2}$, which, according to (1.1), prescribes the relative magnitudes of the settling speed of the individual particles and the descent speed of an equivalent fluid thermal. For $N_c > 1$, the particles were observed to rain out of the cloud as individuals, while for $N_c < 1$, the size and speed of the particle cloud evolves according to the thermal scalings stated in (1.1). Rahimipour & Wilkinson distinguished between three distinct phases of particle cloud motion following release; specifically, a ballistic phase in which the cloud accelerates until attaining a turbulent state, a self-similar turbulent thermal phase, and a dispersive phase, in which the particles have separated from the entrained fluid and settle at w_s. Similar stages were observed by Bühler & Papantoniou (1991), who also attempted to characterize the relatively small spreading rate of the cloud in its dispersive or swarm phase due to the dynamic enhancement of pressure within the cloud. Nakatsuji, Tamai & Murota (1990) examined experimentally two-dimensional (line) particle thermals and demonstrated that the deposition pattern at the bottom of the tank depends critically on the relative magnitudes of the fallout height Z_f and the layer depth H: for $Z_f < H$, a localized deposit arose, while for $Z_f > H$, the particle cloud spreads upon impact, giving rise to a doubly-peaked deposition pattern.

The most extensive experimental study of particle clouds reported to date is that of Ruggaber (2000), who focused on the cloud's thermal phase and demonstrated that it may be subdivided into turbulent and circulating phases. The transition from turbulent to circulating phases is marked by a substantial ($\sim 33\%$) decrease in the entrainment coefficient, from the turbulent value ($\alpha \sim 0.25$) to one consistent with the buoyant vortex ring theory of Turner (1957, 1964). The diminution of entrainment into particle clouds with distance from the source was also quantified by Rahimipour & Wilkinson (1992), who identified the importance of the flow within the thermal on the entrainment coefficient, and so on the fallout height. Noh & Fernando (1993) focused on elucidating the fallout criterion for two-dimensional particle clouds. They concluded that the fallout criterion cannot be simply expressed in terms of a

cloud number, but also depends on the particle Reynolds numbers over the range $0.2 < Re_p < 20$.

Wen & Nacamuli (1996) examined the dependence of the form of particle clouds on the cloud Rayleigh number, defined as $Ra = Q/(w_s^2 b_0^2)$ where b_0 is the initial cloud radius. They report that as Ra is increased, the cloud structure changes from a laminar vortex ring to a turbulent thermal, and finally to a 'wake', which is characterized by a cloud elongated substantially in the direction of motion. They suggest that the entrainment into the cloud is diminished substantially over this progression, and that this large variation may be responsible for much of the discrepancy observed in experimental studies of particle clouds.

Despite its potential environmental significance, the interaction of a particle cloud with a stratified ambient has received very little attention. Luketina & Wilkinson (1994) consider a sediment cloud of initial buoyancy Q settling through a stratified ambient characterized by a constant Brunt–Väisälä frequency N. They observe that the fluid entrained by the sediment cloud sinks to a maximum depth at which the particles fall out, then rebounds to a height, Z_R, at which it intrudes as a gravity current. They develop an accompanying numerical model which demonstrates that the fluid oscillates about Z_R at a frequency comparable to N. Finally, they suggest the importance of the stratified cloud number $N_s = w_s Q^{-1/4} N^{-1/2}$ on the cloud dynamics, noting that the fallout height appears to decrease with N_s. A more detailed investigation of the stratified case is a principal contribution of our paper; in particular, we characterize the explicit dependence of the fallout and rebound heights on N_s through a combined experimental and theoretical approach.

We present herein the results of a combined theoretical and experimental study aimed at elucidating the mixing processes accompanying the settling of particle clouds in homogeneous and stratified ambients. Our theoretical model and numerical simulations are described in § 2. The experimental techniques employed in our study are detailed in § 3. Our study of particle settling in a homogeneous fluid is described in § 4, while the stratified environment is discussed in § 5. The broader relevance and applications of this work are considered in § 6. Particular attention is given to deducing criteria for the various modes of particle deposition from particle clouds in a stratified ambient.

2. Theoretical model

We consider the release of N_p negatively buoyant particles of mass m_p, radius a and density ρ_p into an initially quiescent ambient of density ρ_a. The ambient may either be homogeneous, $\rho_a = \rho_0$, or characterized by a stable linear stratification with a constant Brunt–Väisälä frequency N and density profile $\rho_a(z) = \rho_0(1 + N^2 z)$. Note that z increases with depth from the point of release $z = 0$. The result is a particle cloud with total buoyancy $Q = g' V_0$ defined in terms of the reduced gravity of the particles $g' = (\rho_p - \rho_a)g/\rho_a$, and the initial cloud volume $V_0 = m_p N_p/\rho_p$. The cloud Reynolds number $Re = Ub/\nu$ based on the cloud half-width b and speed U is assumed to be sufficiently large that the cloud initially evolves as a turbulent thermal, entraining ambient fluid as it descends.

Following the entrainment hypothesis (Morton *et al.* 1956), we assume that the horizontal speed of fluid entrainment u into the cloud is proportional to the mean vertical cloud speed w, that is, $u = \alpha w$. Mass conservation thus requires that the total

cloud mass $M = \rho V$ evolves according to

$$\frac{\mathrm{d}M}{\mathrm{d}t} = \frac{\mathrm{d}}{\mathrm{d}t}(\rho V) = \eta 4\pi\alpha\rho_a r^2|w|, \tag{2.1}$$

where η is a shape factor such that the cloud volume is expressed in terms of the maximum (horizontal) cloud radius r by $V = \eta 4\pi r^3/3$. The cloud is thus treated as a slightly oblate ellipsoid with width r and height ηr. Scorer's (1957) and subsequent experimental studies of fluid thermals indicated that $V = 3r^3$; we thus take $\eta = 9/(4\pi)$ in what follows. The mean cloud density is defined as

$$\rho = \frac{\rho_p\phi + \rho_f(1-\phi)}{V}, \tag{2.2}$$

where ρ_f is the mean density of the fluid within the cloud, ϕ is the particle volume fraction and V is the total cloud volume. For a homogeneous ambient, the fluid within the cloud has the same density as the ambient, $\rho_f = \rho_0$, and the cloud buoyancy is independent of z.

In a stratified ambient, the cloud buoyancy is z-dependent and given by

$$Q = \frac{(\rho - \rho_a)Vg}{\rho_a(0)}. \tag{2.3}$$

The rate of change of the ambient density in the cloud's frame of reference, $\mathrm{d}\rho_a/\mathrm{d}t = \rho_a(0)wN^2/g$ may be combined with (2.3) to yield the rate of change of cloud buoyancy:

$$\frac{\mathrm{d}Q}{\mathrm{d}t} = -VwN^2. \tag{2.4}$$

Newton's second law relates the cloud acceleration to the sum of the buoyancy and hydrodynamic forces:

$$\frac{\mathrm{d}}{\mathrm{d}t}\left(wV(\rho + k\rho_a)\right) = \rho_a(0)Q - C_d\rho_a\pi r^2 w^2\frac{w}{|w|}, \tag{2.5}$$

where k and C_d are, respectively, the added mass and drag coefficients of the cloud (Rahimipour & Wilkinson 1992). In their numerical study of particle clouds in a stratified ambient, Luketina & Wilkinson (1994) examined a similar set of equations, and set $C_d = 1/2$ and $k = 1/2$, values appropriate for a rigid sphere at high Reynolds number; however, experimental studies suggest significantly smaller values. Maxworthy's (1974) observations of turbulent vortex rings suggest a value of 0.02 for C_d. Ruggaber's (2000) study of particle clouds actually suggested small negative values for both C_d and k, from which he concluded that the appropriate values must be negligibly small. In § 4.2, we infer values of C_d and k by comparing our simulations and experimental observations of the descent rates of particle clouds; the results so deduced are consistent with those deduced by Maxworthy (1974) and Ruggaber (2000).

Equations (2.2)–(2.5) are non-dimensionalized using a lengthscale $l_n = Q_0^{1/4}N^{-1/2}$, timescale N^{-1}, and characteristic density $\rho_a(0)$. The non-dimensional equations take the form

$$\frac{\mathrm{d}V}{\mathrm{d}t} = \eta 4\pi\alpha r^2|w|, \qquad \frac{\mathrm{d}Q}{\mathrm{d}t} = -Vw, \qquad \frac{\mathrm{d}z}{\mathrm{d}t} = w, \tag{2.6}$$

$$V\left(\rho_a(1+k) + \frac{\beta Q}{V}\right)\frac{\mathrm{d}w}{\mathrm{d}t} = Q - C_d\rho_a\pi r^2 w^2\frac{w}{|w|} - \beta k w^2 V - \rho_a(1+k)w\frac{\mathrm{d}V}{\mathrm{d}t}, \tag{2.7}$$

where the densities of the ambient and cloud are given by, respectively,

$$\rho_a = 1 + \beta z, \qquad \rho = \rho_a + \beta Q/V, \tag{2.8}$$

and V, Q, w and z now represent non-dimensional variables. The dimensionless number $\beta = Q_0^{1/4} N^{3/2}/g$ indicates the fraction by which the ambient density changes between the release height $z = 0$ and a typical intrusion height, l_n.

The particle fraction in the cloud is given by

$$\phi = \frac{\rho - \rho_a}{\rho_p - \rho_a}, \tag{2.9}$$

and the density of the interstitial fluid in the cloud may be deduced from (2.2):

$$\rho_f = \frac{V\rho - \rho_p \phi}{1 - \phi}. \tag{2.10}$$

When the cloud speed is exceeded by the settling speed of the particles, the particles exit the cloud and so no longer contribute to its negative buoyancy. After fallout, we thus redefine Q to be

$$Q = \frac{(\rho_f - \rho_a)(V - \phi_0 V_0) g}{\rho_a(0)}. \tag{2.11}$$

In a stratified ambient, this reduction of cloud buoyancy Q causes the cloud to ascend to its level of neutral buoyancy, the rebound height.

Numerical simulations of the full system of equations (2.4)–(2.8) were performed using a fourth-order Runge–Kutta integrator. The cloud was started from rest ($w = 0$ at $z = 0$) and owing to our non-dimensionalization, $Q(0) = 1$ by definition. The non-dimensional initial cloud volume is given by $V(0) = V_0 Q_0^{-3/4} N^{3/2}$, and the non-dimensional settling speed corresponds to the stratified cloud number $N_s = w_s Q_0^{-1/4} N^{-1/2}$. Comparison with our experiments was achieved through appropriate choices of β, $V(0)$ and N_s.

In order to test the reliability of our simulations, we first examined the dynamics of negatively buoyant fluid thermals in the absence of particles. In the small β limit that corresponds to a uniform ambient, the similarity solution described by equations (1.1)–(1.2) was well recovered in the limit of small initial cloud volume. In order to further benchmark our numerics, we investigated the behaviour of a negatively buoyant fluid thermal in a stratified ambient. The cloud reaches and overshoots its level of neutral buoyancy Z_N and thereafter oscillates about Z_N. As was the case in the simulations of Luketina & Wilkinson (1994), the period of oscillation about the neutral height is slightly greater than $2\pi N^{-1}$, presumably owing to the influence of entrainment. The intrusion height depends strongly on the numerical value taken for the entrainment coefficient α. In particular, $Z_N N^{1/2}/Q_0^{1/4}$ was 4.04 for $\alpha = 0.15$ and 1.79 for $\alpha = 0.35$. Using the average value, $\alpha = 0.25$, deduced by Scorer (1957) (and in §4.1) yields an intrusion height, $Z_N = 2.79\ Q_0^{1/4} N^{-1/2}$, consistent with the result (1.3) reported by Morton *et al.* (1956). We note that the intrusion height was insensitive to changes in k and C_d, since these parameters influence the cloud speed but not its composition.

Having thus benchmarked our numerical simulations against well-established results in homogeneous and stratified environments, we may proceed by using them to examine the dynamics of particle clouds in both homogeneous and stratified environments. The results of our numerical simulations are presented with our experimental results in §§4 and 5.

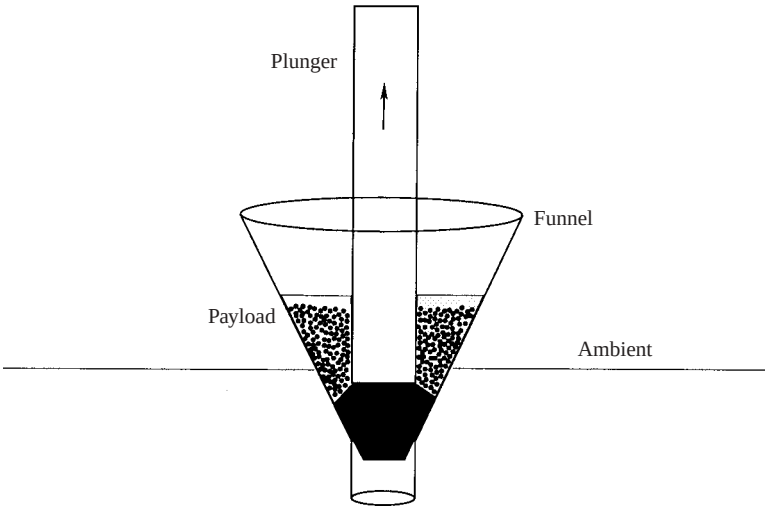

FIGURE 1. A schematic illustration of the release mechanism. The payload consists of known quantities of glass beads, water and fluorescein dye.

3. Experimental technique

A cylindrical tank of diameter 45 cm and depth H = 90 cm was filled with water, or with a linearly stratified saltwater solution using the Oster double-bucket system. The cylindrical tank was housed in a rectangular casing filled with water in order to eliminate parallax. The payload was released by withdrawing a plunger from a funnel in the centre of the tank (figure 1). One of two funnels (of diameters 1.9 cm and 4.4 cm) was used according to the payload size. The release was made precisely at the surface of the water in order to minimize the initial momentum of the cloud. The resulting flow was illuminated from the side by a light sheet, and recorded with a video camera at sufficient distance (3–4 m) to eliminate errors associated with parallax. A grid was placed on the front face of the tank which, together with a timecode generator on the video signal, enabled the computation of cloud speeds. Reviewing the video frames also enabled us to identify the fallout and rebound heights.

The payload contained N_p monodisperse glass spheres of radius a, volume $V_p = 4\pi a^3/3$ and density ρ_p. The properties of the 11 types of particle used (obtained from MO-SCI Corporation) are detailed in table 1. The settling speeds w_s of the individual particles were measured and found to be in good agreement with the empirical relation of Dietrich (1982) for spherical particles:

$$\log W = -3.76715 + 1.92944 \log D - 0.09815 \log D^2 - 0.0057 \log D^3 + 0.00056 \log D^4, \quad (3.1)$$

where $W = w_s^3/g'\nu$, $D = g'a^3/8\nu^2$ and $g' = g(\rho_p - \rho)/\rho$ is the reduced gravity of the particles. For each particle size, five measurements of the settling speed were made, and the observed variance was consistent with that in the particle sizes. The particle Reynolds numbers, $Re = w_s a/\nu$, based on the individual particle settling speeds w_s ranged from 0.15 to 300. Payload masses varied from 0.2 g to 50 g. The payload also contained a small volume (typically 5–10 ml) of water which served to wet the particles completely, and so avoid the delayed onset of turbulence which typically accompanies dry particle releases (Ruggaber 2000). A few drops of dye (either food colouring or fluorescein) were added to the payload in order to facilitate flow visualization by marking the fluid entrained into the particle cloud.

a (cm)	w_s (cm s^{-1})	ρ_p (g cm^{-3})	Re_p
0.1095 ± 0.01	27.4 ± 1.4	2.5	300 ± 40
0.077 ± 0.008	22.0 ± 1.4	2.5	170 ± 25
0.065 ± 0.005	18.2 ± 0.8	2.5	118 ± 12
0.055 ± 0.005	16.4 ± 0.8	2.5	90 ± 12
0.039 ± 0.004	11.3 ± 0.5	2.5	44 ± 6
0.023 ± 0.002	6.6 ± 0.25	2.5	15 ± 2
0.016 ± 0.001	7.7 ± 0.25	4.2	12.3 ± 1.2
0.010 ± 0.001	4.4 ± 0.10	4.2	4.4 ± 0.7
0.005 ± 0.001	1.89 ± 0.05	4.2	0.94 ± 0.2
0.003 ± 0.0005	1.62 ± 0.05	4.2	0.48 ± 0.1
0.002 ± 0.0004	0.78 ± 0.05	4.2	0.15 ± 0.03

TABLE 1. Properties of the glass spheres used in the experiments: radius a, density ρ, measured settling speeds in water w_s and particle Reynolds number $Re_p = w_s a/\nu$.

The virtual origin is defined as the position of the thermal source that would be inferred by extrapolating from its far-field form and assuming that the thermal motion was everywhere self-similar. Deviations of the thermal evolution from a self-similar structure (that is, nonlinear dependence of cloud width on distance from the source) in the vicinity of the origin typically lead to an offset between the real and virtual origins. For example, the delayed onset of turbulence for the case of large payloads of high-density particles typically results in the virtual origin being displaced forward relative to the real origin (and so to a positive virtual origin). In our experiments, a rough estimate of the virtual origin could be obtained by tracing the far-field evolution of the cloud, deducing a mean entrainment coefficient for the cloud in its self-similar thermal phase, and extrapolating backwards. As is typically the case in experimental investigations of turbulent thermals, indeterminacy in the virtual origin and variations in the entrainment coefficient are at once unavoidable and difficult to distinguish, and are the dominant source of scatter in the data.

We assume in the present study that throughout the thermal phase, the particles remain uniformly distributed throughout the cloud. A more detailed consideration of the interaction between the fluid and particle dynamics within the cloud may be found in Ruggaber (2000). Finally, the influence of the domain boundaries was investigated. The entrainment into the plume was significantly reduced when the plume width became comparable to half the tank width. This constraint limited the parameter regime explored in our study.

4. Homogeneous ambient

In all experiments, the cloud Reynolds number $Re = Ub/\nu$ based on the cloud half-width b and speed U was sufficiently large that the fluid motions generated by the sinking cloud were initially turbulent. The cloud Rayleigh number, $Ra = Q/(w_s^2 b_0^2)$ ranged from 20 to 10 000. In accordance with the observations of Rahimipour & Wilkinson (1992), following the release of particles into a homogeneous ambient, the cloud evolved through three distinct phases: the ballistic or acceleration phase; the self-similar thermal phase; and the dispersive phase. While the distinction between the thermal and dispersive phases was readily made, that between the ballistic and thermal phases was less obvious.

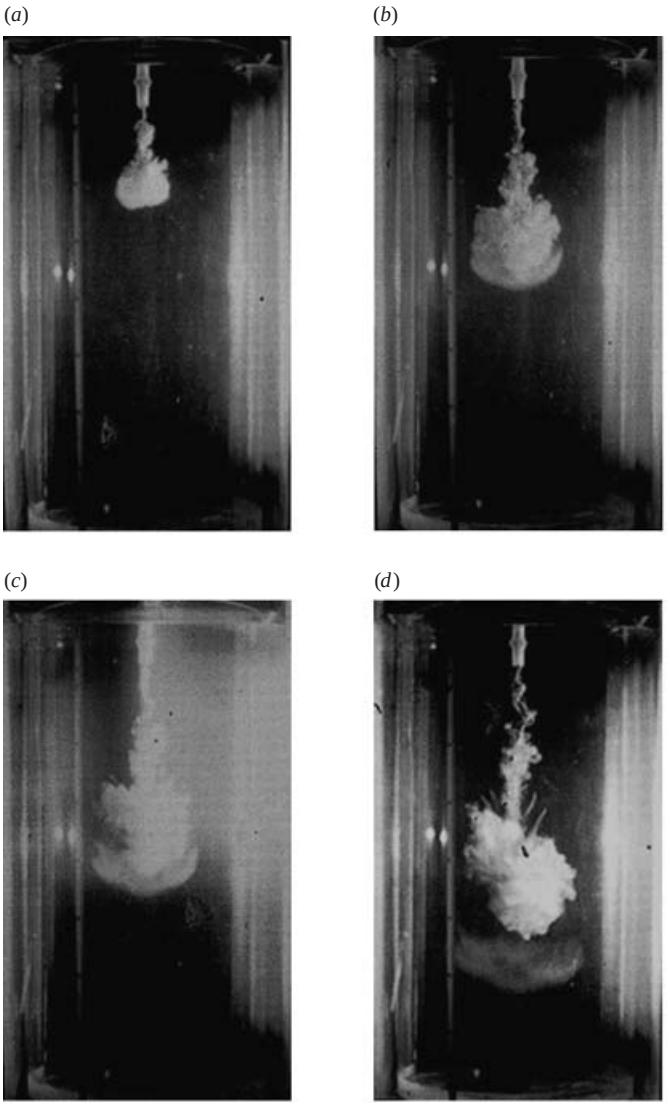

FIGURE 2. The evolution of a turbulent particle cloud in a homogeneous ambient. The cloud grows through turbulent entrainment (a, b) until the particles fall out of the cloud in the form of a bowl-shaped swarm (c, d). The fluid entrained by the cloud is rendered visible by adding fluorescein dye to the initial payload.

Figure 2 illustrates the typical evolution of a particle cloud in a homogeneous environment. The thermal form is taken after a brief adjustment phase, and persists until the particles begin to precipitate out of the bottom of the cloud. Subsequently, the particles descend in the form of a bowl-shaped swarm within which there is negligible relative motion between the particles. The fallout arises when the particles can no longer be suspended by the circulation within the cloud. The bowl shape may be understood in terms of the interaction between the vortical flow within the cloud and the relatively dense suspended sediment: the fallout occurs first along the cloud centreline and last along its edges, where the vortex motion is, respectively, downwards and upwards relative to the cloud. Following fallout, the fluid entrained by the thermal

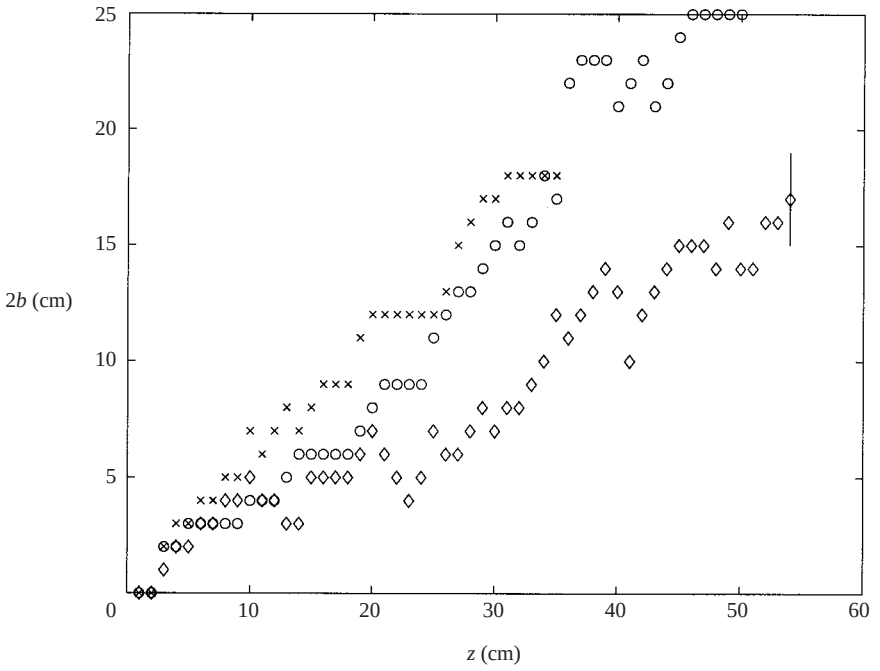

FIGURE 3. Cloud width, $2b$, as a function of the distance of the cloud's centre-of-mass from the source, z, for three payload sizes: ×, 1 g; ○, 7 g; ◇, 20 g. The particle Reynolds number in each experiment is $Re_p = 0.94$. Note that the linear growth characteristic of turbulent thermals is delayed for the largest payload, giving rise to a significant forward displacement of the virtual origin. A characteristic error bar is shown.

trails the particle swarm in the form of a neutrally buoyant vortex ring or momentum puff (Maxworthy 1974, 1977). We note that, while the extent of the adjustment phase appeared to increase with cloud Rayleigh number, the dependence of flow form on Ra reported by Wen & Nacamuli (1996) was not observed. Specifically, the wake regime reported to exist for $Ra > 1000$ was not evident in our experiments with Rayleigh numbers as high as 10 000.

4.1. *Cloud width*

The cloud width is defined as the cloud's maximum horizontal extent, the evolution of which was measured from the video images. Figure 3 indicates the evolution of the cloud width with its mean distance from the source z for three particle clouds prior to fallout. The particle size in each cloud is identical, but the initial cloud mass varies from 1.0 g to 20.0 g. Note that, while the rate of expansion of the cloud ultimately achieves a value independent of payload size (corresponding to $\alpha \sim 0.25$), the distance required to achieve this value is larger for larger payloads: the ballistic phase or zone of flow establishment is extended for larger payloads, leading to a positive virtual origin. In particular, the virtual origin for the 20 g payload is evidently displaced by approximately 10 cm in figure 3. This decreased entrainment in the ballistic phase is consistent with the experimental observations of Baines & Hopfinger (1984), and Rahimipour & Wilkinson (1992). In order to minimize the influence of the displacement of the virtual origin, we typically used payloads between 1 and 10 g.

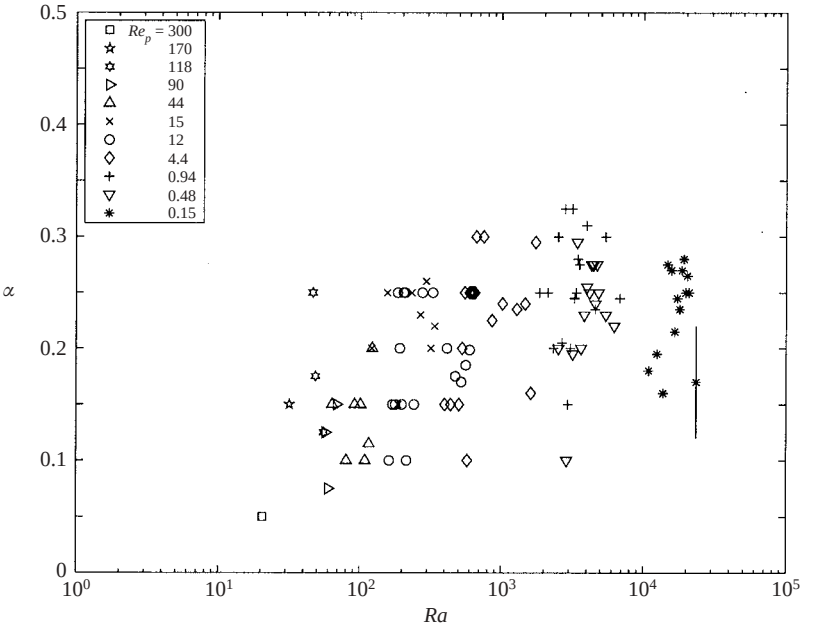

FIGURE 4. The dependence of the entrainment coefficient α on the cloud Rayleigh number $Ra = Q/(w_s^2 b_0^2)$ as defined by Wen & Nacamuli (1996). Values of Re_p for different symbols are given in the key. Characteristic error bars are shown.

Figure 4 indicates the dependence of the entrainment coefficient α on the cloud Rayleigh number defined by Wen & Nacamuli (1996), $Ra = Q/(w_s^2 b_0^2)$, where b_0 is the initial cloud radius. The entrainment rate is calculated from the rate of spread of the thermal once it attains its self-similar phase, that is, following its ballistic phase. The errors reported are associated with the uncertainties inherent in distinguishing between the ballistic and self-similar phases. While a wide range of α values was observed (between 0.1 and 0.3), there was no apparent dependence of α on *Ra*. We conclude that, as for fluid thermals, we may adequately describe the entrainment coefficient as 0.25 ± 0.1. While the explicit dependence of α on cloud number N_c was considered by Rahimipour & Wilkinson (1992) and Ruggaber (2000), for a leading-order description of the particle cloud dynamics, it is sufficient to approximate α by a mean constant value. However, we note that comparison of our experiments and numerics will suggest a weak dependence of α on Re_p.

In the self-similar thermal regime, the cloud width grows linearly with distance from the source. Consequently, the cloud width measured at a particular depth in the tank will be independent of cloud buoyancy provided the cloud is still in its thermal phase. This is clearly evident in figure 5, where the cloud width at, respectively, 30 cm and 50 cm is plotted against cloud buoyancy. Data on the right-hand side of the dashed line correspond to clouds that are still in their thermal phase, and so have a width that is independent of cloud buoyancy. The considerable scatter about the mean is associated with the variability in α and the influence of the adjustment phase on the virtual origin. The data on the left-hand side of the dashed line correspond to clouds which are in their dispersive or swarm phase, and so have a normalized width $2b/z$ that depends explicitly on cloud buoyancy. Note that fewer clouds persist in their thermal phase at $z = 50$ cm.

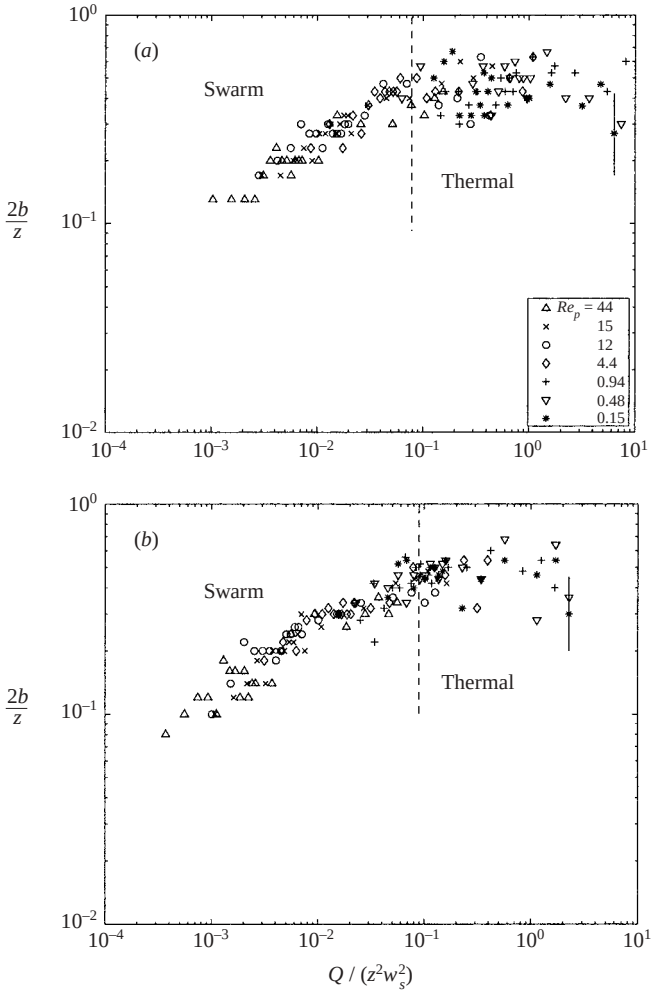

FIGURE 5. The dependence of normalized cloud width $2b/z$ on normalized cloud buoyancy $Q/(z^2 w_s^2)$ at distances (*a*) $z = 30$ cm and (*b*) $z = 50$ cm from the source. On the right-hand side of the dashed line, the clouds are in their thermal phase and $b \sim 0.25z$; on the left-hand side, the clouds are in their swarm phase, and $2b/z$ depends explicitly on Q. Values of Re_p for different symbols are given in the key.

4.2. *Frontal position and cloud speed*

The position of the foremost edge of the cloud, or cloud front Z_M, was evaluated on the video frames and used to compute the cloud speeds. Figure 6(*a*) illustrates the observed dependence of Z_M, on time from release t for three particle clouds with $Re_p = 0.94$. The two distinct dynamic phases of the particle clouds are evident: the thermal phase, in which $Z_M \sim t^{1/2}$ and $U \sim t^{-1/2}$ (as suggested by (1.2)); and the swarm phase, in which $Z_M \sim t$ and $U = w_s$. We note also that the transition from thermal to swarm arises at a fallout height Z_f that increases with payload size.

Tracking the rate of descent of the cloud allows us to infer the hydrodynamic drag and added mass coefficients, respectively, C_D and k, appearing in our theoretical formulation in § 2. Figure 6(*b*) illustrates the descent rate of the 7 g particle cloud (corresponding to the top curve in figure 6*a*) plotted with the results of our numerical

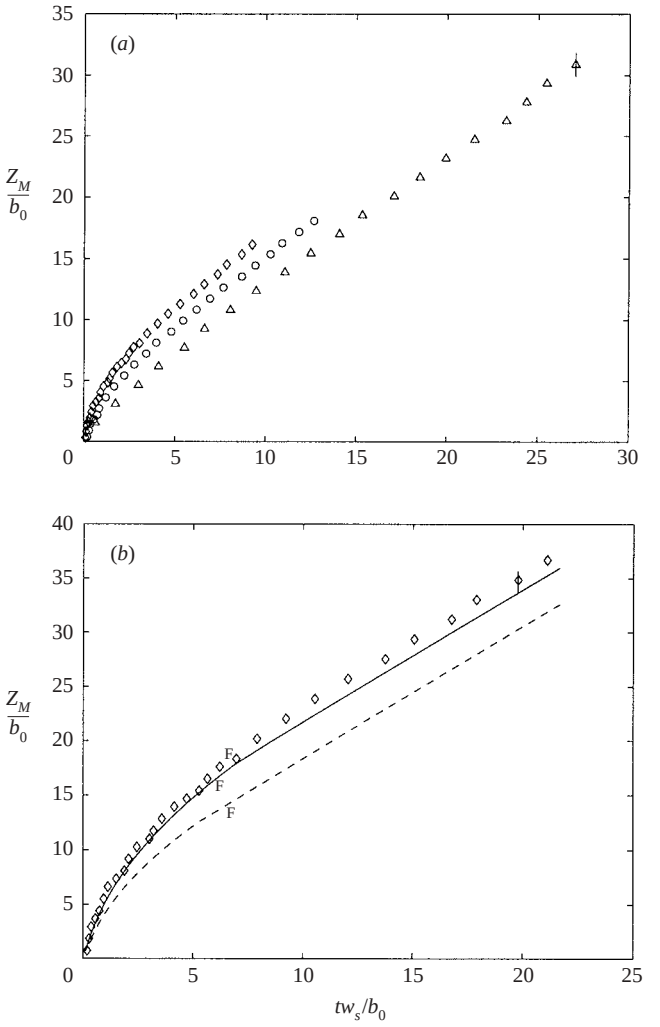

FIGURE 6. (*a*) The dependence of normalized cloud front position Z_M/b_0 on dimensionless time for three payload sizes: △, 1 g; ○, 5 g; ◇, 7 g. In each experiment, $Re_p = 0.94$. After an initial thermal phase in which the cloud speed scales as $t^{-1/2}$ as suggested by (1.2), the particles settle at their individual settling speeds. Note that the larger payloads have a prolonged thermal phase. (*b*) The numerical simulation of the 7 g payload, corresponding to the top curve in (*a*). The dashed line was computed with drag and added mass coefficients $C_d = k = 0.5$ appropriate for a rigid sphere, the solid line with $C_d = 0.02$ and $k = 0$ appropriate for a thermal. F indicates the point of fallout for both the simulations and experiments.

simulations. The dashed line represents the numerical results deduced using the hard-sphere results ($C_d = k = 0.5$) proposed by Luketina & Wilkinson (1994). These results are clearly unsatisfactory: the cloud sinks too slowly, and the fallout height is thus underestimated. The solid line represents the numerical results obtained using the values proposed by Maxworthy (1974) and Ruggaber (2002): $C_d = 0.02$ and $k = 0$. The numerics satisfactorily match the experimental data: the predicted and observed cloud speeds are consistent through both the cloud and swarm phases, and the fallout height is well reproduced. We proceed by adopting the results suggested by

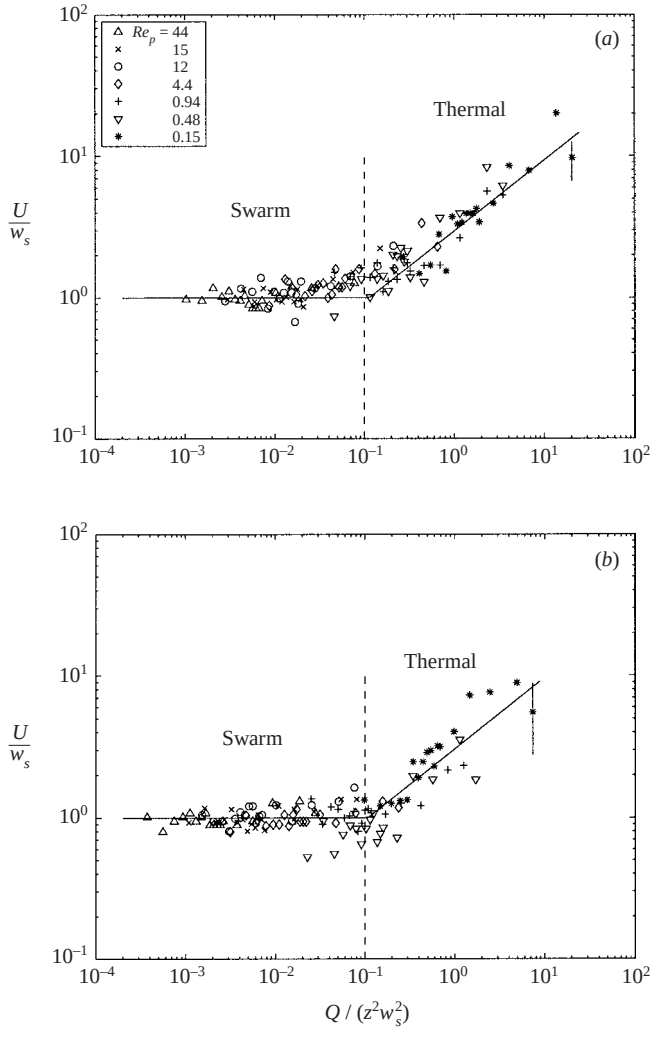

FIGURE 7. The dependence of normalized cloud speed U/w_s on normalized buoyancy $Q/(z^2 w_s^2)$ at (*a*) $z = 30$ cm and (*b*) $z = 50$ cm. On the left-hand side of the dashed line, the clouds are in their swarm phase, and settle at w_s; on the right-hand side, the clouds are in their thermal phase. The numerical simulations yield the solid lines, which have a slope of 0.5 in the thermal phase, where $U \sim Q^{1/2}/z$.

Maxworthy (1974) and Ruggaber (2002), $C_d = 0.02$ and $k = 0$, in all of our numerical simulations of particle clouds.

Figure 7 illustrates the observed cloud speed U measured at two depths, $z = 30$ cm and $z = 50$ cm, as a function of the cloud buoyancy. The cloud speed is normalized by the particle settling speed w_s, so we expect a dependence in the thermal regime of the form

$$\frac{U}{w_s} = C_2 \frac{Q^{1/2}}{z w_s}. \tag{4.1}$$

Two distinct behaviours corresponding to the thermal and swarm regimes are indicated in figure 7. In the thermal regime, the data indicate that the scaling of (4.1) is valid, and that the coefficient $C_2 = (3.0 \pm 0.4)$. In the swarm regime, the speed

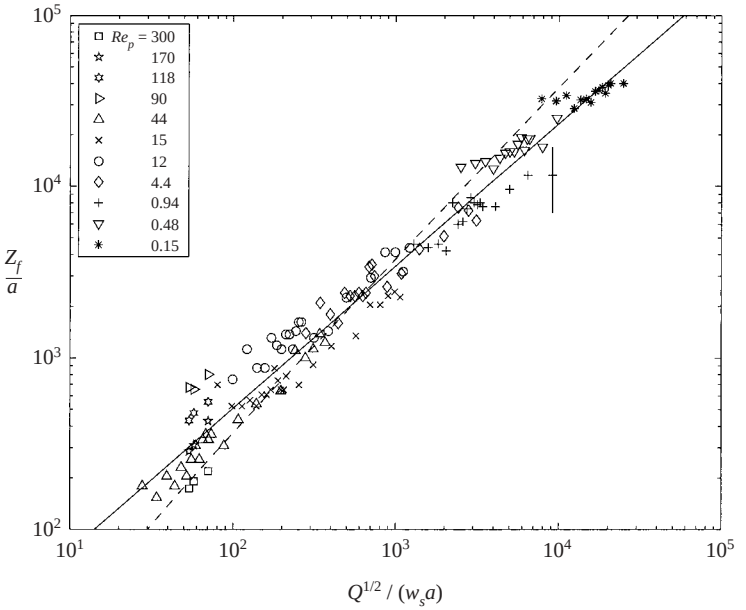

FIGURE 8. The observed dependence of normalized fallout height, Z_f/a, on $Q^{1/2}/w_s a$ for all Re_p considered. The solid line represents the best fit line, which has a slope of 0.83. The dashed line corresponds to the results of our numerical simulations, and has a slope of 1. Values of Re_p for different symbols are given in the key. A characteristic error bar is shown.

is independent of cloud buoyancy, and is comparable to the settling speed of the individual particles. The solid lines correspond to the results of the accompanying numerical simulations, and indicate the dependence of the cloud speeds on height and initial cloud buoyancy. Note that the speed is recorded sufficiently far from the source that it is independent of the cloud's initial volume; consequently, the numerical predictions are independent of particle Reynolds numbers.

4.3. *Fallout height*

Studies of the cloud speed indicate that, in accordance with the conjecture of Bühler & Papantoniou (1991), fallout occurs when the speed of the thermal is matched by the settling speed of the individual particles. This simple physical picture suggests

$$Z_f = C_3 \frac{Q^{1/2}}{w_s}, \tag{4.2}$$

where C_3 is an as yet undetermined coefficient. In our experiments, Z_f was taken to be the cloud depth at which the emergence of the swarm front from the dyed cloud was first apparent. The dependence of Z_f/a on $Q^{1/2}/(w_s a)$ over the entire range of Re_p considered is illustrated in figure 8. The best-fit line indicates a form

$$\frac{Z_f}{a} = (11 \pm 2)\left(\frac{Q^{1/2}}{w_s a}\right)^{5/6}. \tag{4.3}$$

We note that at the lower Re_p, the fallout height increases more slowly with $Q^{1/2}/(w_s a)$ than predicted by the proposed scaling (4.2). A similar Re_p dependence was observed by Noh & Fernando (1993) in their study of line particle clouds, and was attributed to the influence of particle–particle interactions at low Re_p (e.g. Davis & Acrivos 1985).

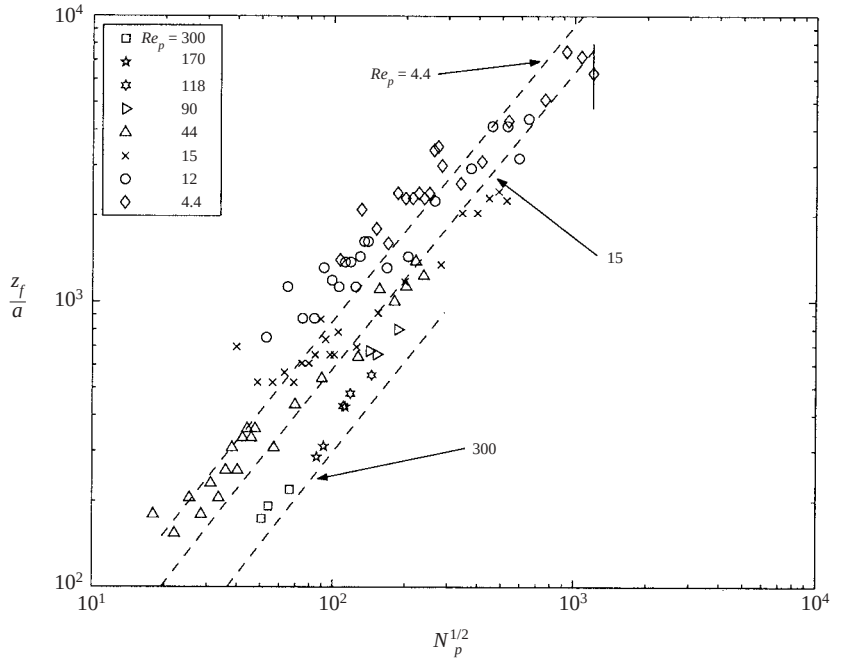

FIGURE 9. The dependence of the fallout height, Z_f, on the number of particles released, N_p, for the case of high-Reynolds-number particles ($Re_p > 4$). The dashed lines indicate the results of our numerical simulations computed with three different Re_p. The offset of the numerical lines reflect the influence of finite initial cloud volume.

The fallout heights computed by our numerical simulations for the parameter range considered in our experiments are presented by the dashed line in figure 8, and indicate a constant $C_3 = 3.66$ in (4.2).

At high Re_p, the settling speed $w_s \sim \sqrt{g'a}$. Substituting for w_s and $Q = g' N_p V_p$ in (4.2) yields the strikingly simple result $Z_f/a \sim N_p^{1/2}$: in the high Re_p regime, the fallout height depends exclusively on the number and size of the particles released. Figure 9 indicates the observed dependence of the fallout height on a and N_p for particle plumes with $4.4 \leqslant Re_p \leqslant 300$, along with the results of our supporting numerical simulations. In both the experiments and numerics, the number of particles was calculated from the initial cloud buoyancy, particle size and density (table 1). In the numerics, the initial cloud buoyancy was varied over a range corresponding to those examined experimentally, and three particle sizes were chosen to correspond to particle Reynolds numbers of $Re_p = 4.4$, 15 and 300. The slopes of the three resulting lines are seen to be identical and equal to 1 in accordance with the anticipated scaling (4.4). The numerics indicate that the spread in the data results from the wide range of Re_p considered. The increasing initial cloud volume and concomitant departure from the similarity solution for the larger particles results in relatively small values of Z_f/a. Nevertheless, the numerics and experiments both serve to validate the proposed scaling, and indicate that the data may be described to leading order by

$$Z_f = (9 \pm 2)\, a N_p^{1/2}. \tag{4.4}$$

In the parameter regime $1 < Re_p < 10$, Rahimipour & Wilkinson (1992) observed that the transformation from thermal to swarm arises at a critical cloud number,

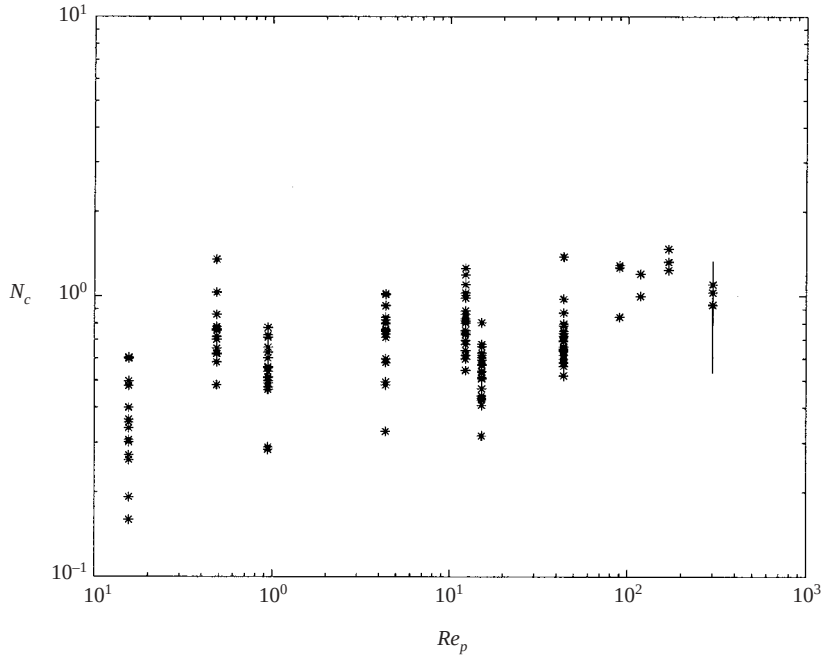

FIGURE 10. Dependence of cloud number at fallout $N_c = w_s b/Q^{1/2}$ on particle Reynolds number, $Re_p = w_s a/\nu$. A characteristic error bar is shown.

$N_c = w_s b/Q^{1/2} = 1$. Figure 10 indicates the dependence of the critical cloud number on Re_p in our experimental study. Over a substantially wider parameter regime, $0.1 < Re_p < 300$, our observations substantiate the importance of a cloud number criterion for particle fallout, and indicate a mean critical cloud number of 0.8. This value is consistent with our inferred values of C_3 in (4.2) and the entrainment coefficient; specifically, $N_c \approx \alpha C_3$. Finally, we note that as Re_p increases, the critical cloud number increases and approaches unity, a trend which again suggests the importance of particle–particle interactions at low Re_p.

5. Stratified ambient

We proceed by describing the influence on the particle cloud dynamics of a stable ambient stratification. We again denote by z the distance from the source $z = 0$ and assume that the ambient has a linear density profile, $\rho(z) = \rho_0(1 + N^2 z/g)$. The settling speed w_s and cloud buoyancy are defined at $z = 0$ where $\rho = \rho_0$; the vertical density variations are assumed to be sufficiently small that w_s does not vary substantially through the fluid domain. The uniform stratification introduces an additional lengthscale into the problem, namely $Q^{1/4}N^{-1/2}$, which in the case of a fluid thermal prescribes the intrusion height Z_N via (1.3). The nature of the sedimentation from a particle cloud in a stratified ambient depends critically on the magnitude of the stratified cloud number $N_s = w_s Q^{-1/4} N^{-1/2}$ (Luketina & Wilkinson 1994), which prescribes the relative magnitudes of the Brunt–Väisälä period, $1/N$, and the time required for an individual particle to fall a distance Z_N.

The flow evolution for the case of $N_s > 1$ is illustrated in figure 11. The initial phase is similar to that arising in a homogeneous ambient: the cloud descends as a turbulent thermal until reaching its fallout height, beyond which the particles descend

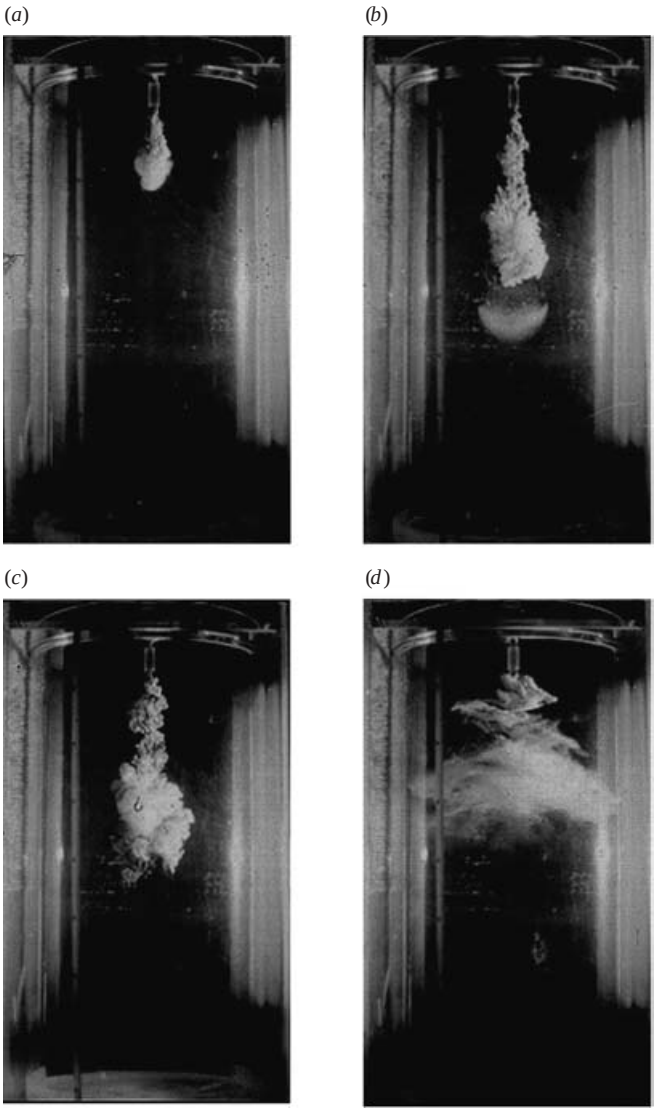

FIGURE 11. A particle cloud settling in a stratified ambient for stratified cloud number $N_s > 1$. The cloud evolution is similar to that in a homogeneous environment (*a*) until particle fallout (*b*); subsequently, the entrained fluid ascends (*c*) to a rebound height Z_R, where it intrudes as a neutral cloud (*d*).

in the form of a bowl-shaped particle swarm. Following particle fallout, the fluid contained within the cloud descends some distance owing to its inertia, then ascends and oscillates vertically at a frequency corresponding closely to N before intruding at its rebound height Z_R. The evolution of the flow for the case of $N_s < 1$ is illustrated in figure 12. The particle cloud initially descends as a turbulent thermal, then overshoots, rebounds past, and intrudes at its neutral buoyancy Z_N as an axisymmetric particle-laden gravity current. The particles fall out over the range of heights between the point of maximum penetration of the cloud and Z_N. Particles released from the neutral cloud spread in an irregular fashion, and over a relatively broad area; we thus

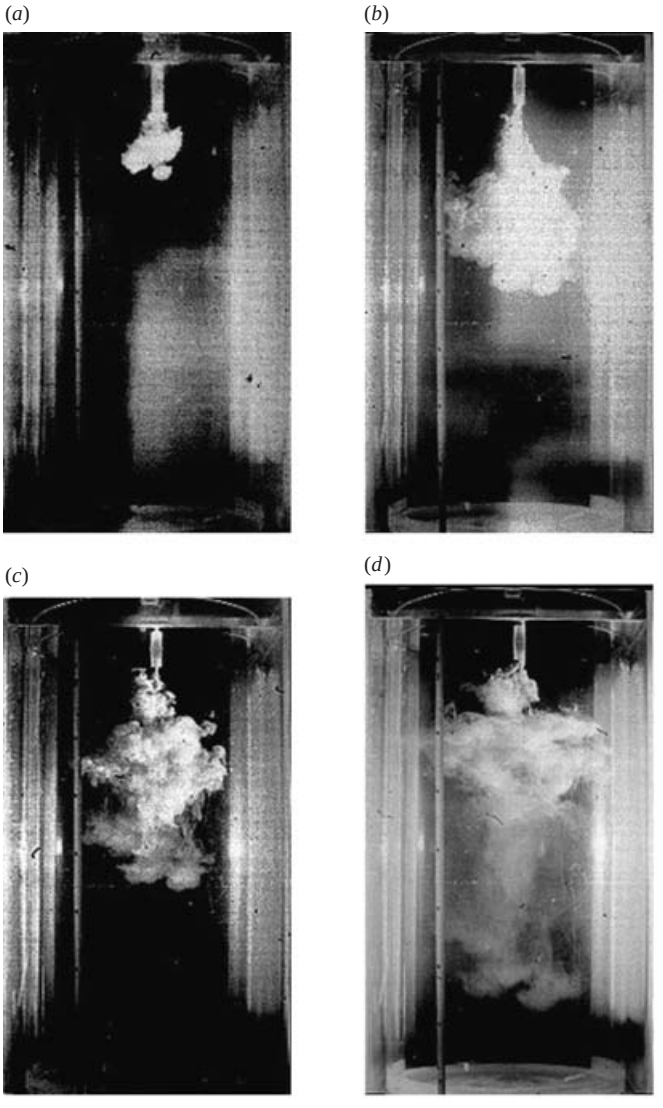

FIGURE 12. A particle cloud settling in a stratified ambient for $N_s < 1$. The cloud descends to its level of neutral buoyancy, where it intrudes and the particles settle out in an irregular fashion. Subsequently, the entrained fluid ascends to a rebound height Z_R, where it intrudes as a neutral cloud.

refer to this mode of sedimentation as a 'dispersed' fallout. As the particles settle out, the fluid in the neutral cloud again ascends some distance, oscillates then intrudes at its rebound height Z_R.

Dimensional analysis indicates that fallout in the stratified ambient must be uniquely characterized in terms of two dimensionless groups, $Z_f/Z_N \sim Z_f N^{1/2} Q^{-1/4}$ and $N_s = w_s Q^{-1/4} N^{-1/2}$, the stratified cloud number. Figure 13 illustrates the observed dependence of the fallout height on the stratified cloud number. For $N_s < 1$, the particles fall out over the range of depths between the maximum depth of penetration and the neutral height expected for an equivalent fluid thermal $Z_N = (2.6 \pm 0.4) Q^{1/4} N^{-1/2}$. For the small N, large N_s limit, we expect the fallout to be

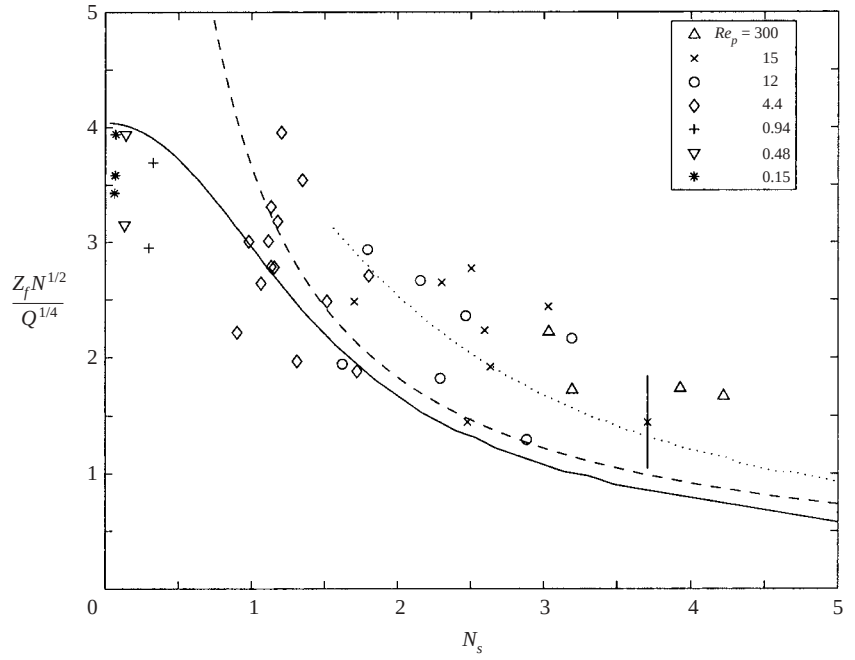

FIGURE 13. The dependence of the fallout height, Z_f, on the stratified cloud number, $N_s = w_s Q^{-1/4} N^{-1/2}$, for particle clouds in a stratified ambient. For $N_s < 1$, the particles fall out between the neutral height of the equivalent fluid thermal, $Z_N = (2.6 \pm 0.4)\ Q^{1/4} N^{-1/2}$ and the depth of maximum penetration. For $N_s > 2$, the particles fall out at a height $Z_f < Z_N$ as in a homogeneous environment. The numerical results are denoted by a solid line. For large N_s, the influence of stratification is negligible, and the fallout height is given by the homogeneous result (4.2) (dashed line). The discrepancy between the numerics and theory suggests reduced entrainment coefficients for the large Re_p particles; the dotted line indicates the results of numerics with $\alpha = 0.17$, the mean value appropriate for $12 < Re_p < 44$, as suggested by figure 4.

uninfluenced by the ambient stratification and so to arise at a height appropriate for a homogeneous ambient. The dashed line in figure 13 corresponds to the homogeneous fallout height (4.2) with a value of $C_2 = 3.77$ appropriate for the corresponding particle sizes.

The computed dependence of the fallout height on the stratified cloud number appears in figure 13 as a solid curve. The numerical simulations indicate that the crossover from the stratified to the homogeneous fallout height should arise at approximately $N_s = 2$. A plausible explanation for the discrepancy between the numerics and experiments evident in figure 13 is a weak dependence of the entrainment coefficient α on the particle size, as is evident from figure 4, where α is seen to decrease weakly with increasing Re_p. A smaller entrainment coefficient implies that the cloud buoyancy is reduced relatively slowly: the cloud thus travels faster, and the fallout height increases. This trend is evident in the homogeneous results of figure 8: smaller and larger particles have fallout heights that are systematically lower and higher, respectively, than would arise if the entrainment coefficient were independent of particle Reynolds number. A similar trend can be observed in the experiments of Noh & Fernando (1993). In figure 13, the numerical simulations thus systematically underpredict the fallout heights of the larger particles (larger N_s values).

The dashed line in figure 13 indicates the fallout heights predicted numerically with an entrainment coefficient of $\alpha = 0.17$, the mean value appropriate for $12 < Re_p < 44$ indicated by figure 4. This discrepancy underlines the need for further investigation of the factors influencing the magnitude of the entrainment into particle clouds. However, even with a constant value of $\alpha = 0.25$, our model yields general agreement with the experimental data.

5.1. *Rebound height*

The fate of the fluid that comes into contact with the particulate matter may have considerable environmental significance if the particulate matter is contaminated. When the particles fall out of the cloud in a stratified ambient, the fluid comprising the cloud is buoyant relative to the ambient, and so ascends to its rebound height at which it intrudes. We here present a simple calculation which yields a new relation between the rebound and fallout heights.

The volume of the cloud, $V(z)$, in the thermal regime is given by

$$V(z) = C_4 \alpha^3 z^3, \tag{5.1}$$

where C_4 is a constant shape factor, and we assume that the cloud is sufficiently far from the point of release that V_0 is negligible. The rate of change of the total mass of the thermal, $M(z)$, with depth is given by

$$\frac{\mathrm{d}M}{\mathrm{d}z} = \rho(z)\frac{\mathrm{d}V}{\mathrm{d}z} = C_4 3\alpha^3 z^2 \rho_0 \left(1 + \frac{N^2}{g} z\right). \tag{5.2}$$

Integration yields the evolution of the mass of the particle cloud in its thermal phase:

$$M(z) = M_0 + \int_{z=0}^{z} \frac{\mathrm{d}M}{\mathrm{d}z}\,\mathrm{d}z = M_0 + C_4 3\alpha^3 \rho_0 \left(\frac{z^3}{3} + \frac{N^2 z^4}{4g}\right). \tag{5.3}$$

The density of the cloud fluid at a height z is thus given by

$$\rho(z) = \frac{M(z) - M_0}{V(z)} = \frac{3C_1 \alpha^3 \rho_0 (z^3/3 + N^2 z^4/(4g))}{C_4 \alpha^3 z^3}. \tag{5.4}$$

The excess density of the fluid component of the thermal is thus three-quarters that of the local ambient:

$$\rho(z) = \rho_0 \left(1 + \frac{3N^2}{4g} z\right). \tag{5.5}$$

This simple dependence allows us to relate the rebound height to the fallout height. Assuming that the cloud fluid that remains following fallout does not mix with the ambient during its ascent, it should rebound to, and intrude at, a height

$$Z_R = \tfrac{3}{4} Z_f. \tag{5.6}$$

While Luketina & Wilkinson (1994) did not present their data in such a way that we can infer the relative magnitudes of Z_R and Z_f in their experiments, it is noteworthy that the one experiment presented in their figure 2 is reasonably well described by relation (5.6).

In our experiments, Z_R was taken as the mean height of the neutral cloud resulting from the intrusion of the rebounded fluid, while $Z_f^0 = (1 + \alpha\eta) Z_f$ was taken as the base of the cloud at fallout. Our leading-order result (5.7) thus may be re-expressed

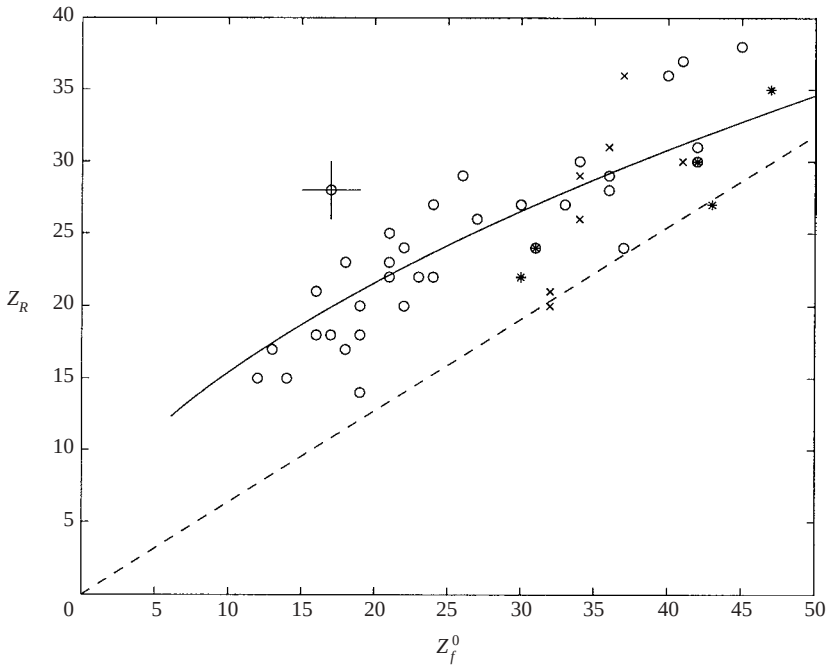

FIGURE 14. The dependence of the rebound height, Z_R, on the fallout height, Z_f^0, for particle clouds in a stratified ambient. ○, a bowl fallout ($N_s > 1$); ×, a dispersed fallout ($N_s < 1$); *, the intermediate case ($N_s \sim 1$). The dashed line represents the theoretically predicted $Z_R = 3Z_f/4 \approx 0.63Z_f^0$. The solid line indicates the results of the numerical simulations, which consider the influence of entrainment after fallout. Particle Reynolds numbers ranged from 0.15 to 44. Characteristic error bars are shown.

as

$$Z_R = \tfrac{3}{4}Z_f = \tfrac{3}{4}\frac{1}{1+\alpha\eta}Z_f^0 \;\approx\; 0.63Z_f^0. \tag{5.7}$$

This relation between the rebound and fallout height appears as the dashed line in figure 14 along with the the observed relation between the fallout and rebound heights for both bowl and dispersed fallouts. The fact that Z_R typically exceeds the predicted value of $3Z_f/4 = 0.63Z_f^0$ is consistent with the rebounding cloud entraining relatively dense fluid as it overshoots Z_f, then ascends. We thus use our numerical model to investigate the influence of entrainment following fallout. We expect that, as the cloud overshoots then rebounds, it will entrain, but that, owing to reduced cloud speeds, the entrainment coefficient α may be diminished. The case of no entrainment $\alpha = 0$ reproduces the theoretical prediction (5.7), and is represented by the dashed curve in figure 14. The case of $\alpha = 0.25$ is represented by the solid curve which agrees well with our data. Our results thus indicate that $\alpha = 0.25$ is a good estimate even as the cloud overshoots then ascends to its rebound height.

6. Discussion

We have described the mixing processes accompanying the descent of particle clouds in homogeneous and stratified fluids. In the homogeneous ambient, following an initial ballistic phase, the particle cloud descends as a thermal until reaching its fallout height, Z_f, where the particles settle out of the cloud in the form of a

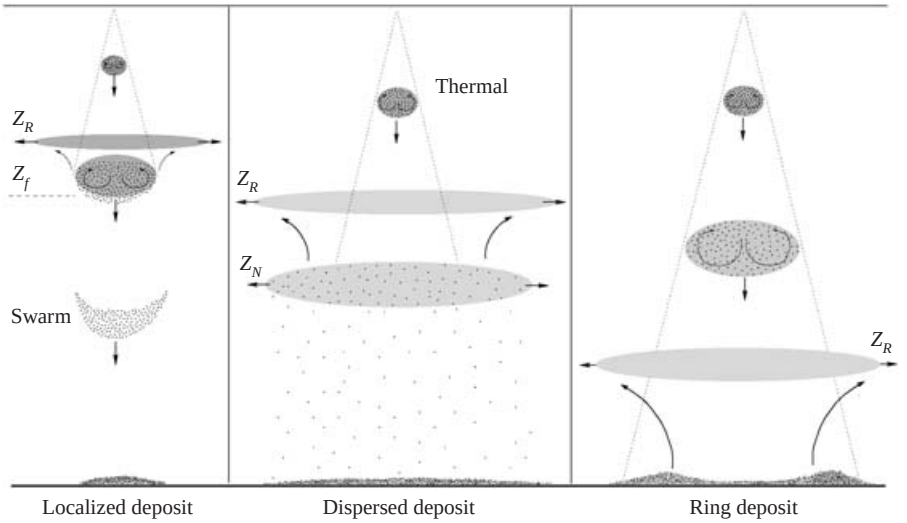

FIGURE 15. A schematic illustration of the three possible scenarios accompanying particle settling in a stratified ambient of depth H: (*a*) the particles fall out before the cloud reaches its level of neutral buoyancy, thus giving rise to a localized deposit; (*b*) the cloud reaches its level of neutral buoyancy before fallout, thus giving rise to a relatively dispersed deposit; (*c*) the cloud retains its thermal form throughout its descent, collides with the lower boundary, and gives rise to a ring-shaped deposition pattern.

bowl-shaped swarm. After fallout, the entrained fluid descends behind the particle swarm in the form of a neutrally buoyant vortex ring.

In contrast with the observations of Wen & Nacamuli (1996), we have not observed a significant dependence of flow form on the cloud Rayleigh number. In particular, the wake regime reported by Wen & Nacamuli (1996) for $Ra > 1000$ was not observed in our experiments even at $Ra = 10\,000$. We have seen that increasing Ra serves at once to extend the zone of flow establishment and diminish the initial entrainment into the particle cloud. While it is difficult to speculate on the reason for this discrepancy, one plausible explanation for the appearance of the wake structure in the experiments of Wen & Nacamuli (1996) was that the adjustment phase of their clouds persisted throughout the cloud descent. Other possibilities include a sizeable range of source particles, and that their particles were subject to an interactive force. This latter possibility seems particularly likely given that the wake structure they report is precisely that assumed by particle clouds comprised of clays which are known to flocculate.

The form of particle deposition from a discrete release of particles in a stratified fluid depends on the relative magnitudes of the layer depth H, the fallout height Z_f and the intrusion height of an equivalent fluid thermal, Z_N. The three possible scenarios are illustrated in figure 15. For $N_s > 1$, the particles will fall out of the cloud before it attains its neutral height, descend as a swarm with limited spread beyond the fallout height (Bühler & Papantoniou 1991), and so give rise to a localized deposit. The fluid entrained by the particle cloud will ascend and intrude at a rebound height somewhat greater than $3Z_f/4$. For $N_s < 1$, the particles settle out in an irregular fashion at a depth between Z_N and the maximum penetration depth, thus giving rise to a relatively distributed deposit. The entrained fluid will again ascend to, and intrude at, a height slightly greater than $3Z_N/4$. When the particles fall out from the base of

		Localized deposit	Dispersed deposit	Ring deposit
Homogeneous environment	$Re_p > 0.15$	$Q < \frac{(w_s a)^2}{312}\left(\frac{H}{a}\right)^{6/5}$	NA	$Q > \frac{(w_s a)^2}{312}\left(\frac{H}{a}\right)^{6/5}$
	$Re_p > 4$	$N_p < \frac{1}{81}\left(\frac{H}{a}\right)^{2}$	NA	$N_p > \frac{1}{81}\left(\frac{H}{a}\right)^{2}$
Stratified environment	$N_s < 1$	NA	$Q < \frac{1}{6} H^4 N^2$	$Q > \frac{1}{6} H^4 N^2$
	$N_s > 2$	$H > 3.5\frac{Q^{1/4}}{N^{1/2}} - 0.5\frac{w_s}{N}$	NA	$H < 3.5\frac{Q^{1/4}}{N^{1/2}} - 0.5\frac{w_s}{N}$

TABLE 2. Criteria for the three modes of particle deposition: a localized deposit, a dispersed deposit, and a ring deposit arising from the cloud colliding with the bottom prior to fallout. Both homogeneous and stratified ambients are considered. Criteria are expressed in terms of the initial cloud buoyancy Q, particle radius a, fluid viscosity ν, layer depth H, reduced gravity of the particles g' and Brunt–Väisälä frequency N. For large N_s, the homogeneous criteria become relevant. NA denotes 'not applicable'.

the spreading neutral cloud, they may not settle as individuals; rather, a convective instability initiated at the base of the cloud may prompt the emergence of microscale particle-laden plumes. Consequently, the dynamics of convective sedimentation from a gravity current (Maxworthy 1999; de Rooij, Linden & Dalziel 1999) will play an important role in determining the subsequent rate and form of particle settling and deposition.

Finally, for either homogeneous or stratified ambients, if $H < Z_f$, the cloud will maintain its thermal form throughout its descent. Consequently, it will collide with the lower boundary as a turbulent vortex ring. The relevant dynamics is expected to be similar to that of atmospheric microbursts (Linden & Simpson 1985), in which vortex stretching in the expanding vortex ring may generate high flow speeds. In the context of particle clouds dumped at sea, one expects that such vigorous motions may lead to scouring and resuspension of particulate material from the sea floor, and will lead to a ring-shaped deposit. This scenario has been observed in the two-dimensional study of Nakatsuji *et al.* (1990), and is presumably responsible for the doubly peaked deposition pattern on the seafloor following the dumping of dredged material at sea (Mutoh, Yoshei & Ishida 1974). In a stratified ambient, the height of ascent of the cloud fluid following particle settling will depend on the entrainment induced following touchdown. If this entrainment is negligible, the fluid will ascend to a depth of $3H/4$. The dynamics of a turbulent particle cloud colliding with a rigid boundary, and the resulting pattern of deposition, is left as a subject for future study.

Our study thus yields criteria, summarized in table 2, for three distinct modes of particle deposition from a particle cloud comprised of either high or low *Re* particles in a homogeneous or stratified environment. Note that the dispersed deposit can arise exclusively in the stratified environment. As a caveat, we note that other physical processes may be important in the dumping of solid material, for example, polydispersity in the source particles, and particle clumping or flocculation in clays, muds and other chemically active particles (Wen & Nacamuli 1996). Moreover, while our experimental study has yielded robust scalings describing the dynamics of particle clouds and their subsequent deposition patterns, it has also underlined

the indeterminacy in the numerical coefficients introduced by the influence of the ballistic phase and the variability of the entrainment coefficient. In suggesting a weak dependence of α on Re_p such as that evident in the study of Noh & Fernando (1993), our study motivates further experimental studies of the factors influencing entrainment into particle clouds. Other factors influencing the source conditions (e.g. whether the particulate matter is wet or dry) may have an additional influence on delaying the onset of self-similar cloud behaviour (Ruggaber 2000).

Finally, we have presented a system of ordinary differential equations describing particle cloud dynamics in homogeneous and stratified ambients that allow for efficient numerical simulation. The numerics have served to validate and determine the limitations of our leading-order results deduced from simple theory and scaling arguments. The numerical model may be readily extended to describe more complex physical situations; for example, payloads composed of polydisperse particles, or particles that react with the environment. Such extensions will be the subject of future consideration.

J.B. gratefully acknowledges support from an NSF Career Grant CTS-0130465. F.B. was supported in part by a PSG-B fellowship from NSERC. B.T. was supported by MIT's Undergraduate Research Opportunity Program.

REFERENCES

Baines, W. D. & Hopfinger, E. J. 1984 Thermals with large density difference. *Atmos. Environ.* **18**, 1051–1057.

Bradley, W. H. 1965 Vertical density currents. *Science* **150**, 1423–1428.

Bühler, J. & Papantoniou, D. A. 1991 Swarms of coarse particles falling through a fluid. In *Environmental Hydraulics* (ed. J. T. Lee & T. K. Cheung), pp. 135–140. Balkema, Rotterdam.

Bühler, J. & Papantoniou, D. A. 1999 Barge dumping of rubble in deep water. In *Environmental Hydraulics* (ed. J. H. W. Lee, A. W. Jayawardena & Z. Y. Wang), pp. 193–198. Bulkema, Rotterdam.

Davis, R. H. & Acrivos, A. 1985 Sedimentation of noncolloidal particles at low Reynolds numbers. *Annu. Rev. Fluid Mech.* **17**, 91–118.

Dietrich, W. 1982 Settling velocity of natural particles, *Water Resources Res.* **18**, 1615–1626.

Escudier, M. P. & Maxworthy, T. 1973 On the motion of turbulent thermals. *J. Fluid Mech.* **61**, 541–552.

Linden, P. F. & Simpson, J. E. 1985 Microbursts: a hazard for aircraft. *Nature* **317**, 601–602.

Luketina, D. & Wilkinson, D. 1994 Particle clouds in density stratified environments. *Proc. 4th Symp. of Stratified Flows, Grenoble, France.*

Maxworthy, T. 1974 Turbulent vortex rings. *J. Fluid Mech.* **64**, 227–39.

Maxworthy, T. 1977 Some experimental studies of vortex rings. *J. Fluid Mech.* **81**, 465–95.

Maxworthy, T. 1999 The dynamics of sedimenting surface gravity currents. *J. Fluid Mech.* **392**, 27–44.

Morton, B. R., Taylor, G. I. & Turner, J. S. 1956 Turbulent gravitational convection from maintained and instantaneous sources. *Proc. R. Soc. Lond.* **234**, 1–23.

Mutoh, S., Yoshii, S. & Ishida, T. 1974 Sand heap undulation on the sea bed by the bottom-dump barge for large-scale land reclamation. *Tech. Rep. Mitsubishi Heavy Industry* **11** (1), 92–104.

Nakatsuji, K., Tamai, M. & Murota, A. 1990 Dynamic behaviours of sand clouds in water. *Intl Conf. on Physical Modelling of Transport and Dispersion, MIT, Cambridge,* 8C, pp. 1–6.

Noh, Y. & Fernando, H. J. S. 1993 The transition in the sedimentation pattern of a particle cloud. *Phys. Fluids* A **5**, 3049–3055.

Papantoniou, D., Bühler, J. & Dracos, T. 1990 On the internal structure of thermals and momentum puffs. *Intl Conf. on Physical Modelling of Transport and Dispersion, MIT, Cambridge*, 4A, pp. 31–36.

Rahimipour, H. & Wilkinson, D. 1992 Dynamic behaviour of particle clouds. *11th Australasian Fluid Mech. Conf. University of Tasmania, Hobart, Australia*, pp. 743–746.

Richards, J. M. 1961 Experiments on the penetration of an interface by buoyant thermals. *J. Fluid Mech.* **11**, 369–384.

de Rooij, F., Linden, P. F. & Dalziel, S. B. 1999 Saline and particle-driven interfacial intrusions. *J. Fluid Mech.* **389**, 303–334.

Ruggaber, G. J. 2000 The dynamics of particle clouds related to open-water sediment disposal. Ph.D. thesis, Department of Civil and Environmental Engineering, MIT.

Scorer, R. S. 1957 Experiments on convection of isolated masses of buoyant fluid. *J. Fluid Mech.* **2**, 583–594.

Slack, G. W. 1963 Sedimentation of a large number of particles as a cluster in air. *Nature* **200**, 1306.

Socolofsky, S. A., Crounse, B. C. & Adams, E. E. 1999 Multi-phase plumes in uniform, stratified, and flowing environments. *Environmental Fluid Mechanics – Theories and Applications* (ed. H. Shen, A. Cheng, K.-H. Wang & M. H., Teng).

Turner, J. S. 1957 Buoyant vortex rings. *Proc. R. Soc.* A **239**, 61–75.

Turner, J. S. 1964 The dynamics of spheroidal masses of buoyant fluid. *J. Fluid Mech.* **19**, 481–90.

Turner, J. 1973 *Buoyancy Effects in Fluids*. Cambridge University Press.

Wen, F. & Nacamuli, A. 1996 The effect of the Rayleigh number on a particle cloud. *Hydrodynamics* (ed. A. T. Chwang, J. H. W. Lee & D. Y. C. Leung), pp. 1275–1280.

Woodward, B. 1959 The motion in and around isolated thermals. *Q. J. R. Met. Soc.* **85**, 144–151.